

## NEW METHOD FOR CONSTRUCTING A VISIBILITY GRAPH-NETWORK IN 3D SPACE AND A NEW HYBRID SYSTEM OF MODELING

Matej BABIČ

*Jozef Stefan Institute  
Jamova cesta 39  
Ljubljana, Slovenia  
e-mail: babicster@gmail.com*

Ladislav HLUCHY, Peter KRAMMER

*Institute of Informatics  
Slovak Academy of Sciences  
Dúbravská cesta 9  
845 07 Bratislava, Slovakia  
e-mail: Ladislav.Hluchy@savba.sk, peter.krammer@gmail.com*

Branko MATOVIČ

*Vinča Institute of Nuclear Sciences  
Department of Materials Science  
P. O. Box 522  
11001 Belgrade, Serbia  
e-mail: mato@vinca.rs*

Ravi KUMAR

*Department of Metallurgical and Materials Engineering,  
and Central XRD Laboratory  
Indian Institute of Technology-Madras (IIT Madras)  
Chennai 600036, INDIA  
e-mail: nvrk@iitm.ac.in*

Pavel KOVAČ

*Faculty of Technical Sciences, University of Novi Sad  
Trg Dositeja Obradovića 6  
Novi Sad, Serbia  
e-mail: pkovac@uns.ac.rs*

**Abstract.** This paper describes a new method for constructing a visibility graph in 3D space. We use a method for predicting porosity of hardened specimens. We also use an intelligent system method to predict porosity of hardened specimens. Visibility graphs have many applications, one of which is the analysis of trend lines of market graphs. It is possible to use 2D visibility graphs for such analysis and the construction for 2D visibility graphs is well known; however, in this paper, we will present a new method for the construction of 3D visibility graphs. 3D visibility computations are central to any computer graphics application. Drawing graphs as nodes connected by links in 3D space is visually compelling but computationally difficult. Thus, the construction of 3D visibility graphs is highly complex and requires professional computers or supercomputers. This article describes a new method for analysing 3D visibility graphs. We develop new method for draws 3D visibility graphs for analysing microstructure pictures of robot laser-hardened specimens. The microstructure of robot laser-hardened specimens is very complex; however, we can present it using 3D visibility graphs. New method for the construction of 3D visibility graphs is very useful in many cases, including: illumination and rendering, motion planning, pattern recognition, computer graphics, computational geometry and sensor networks and the military and automotive industries. We use this new algorithm for determination complexity of porosity of the microstructure of robot laser-hardened specimens. For predicting surface porosity of hardened specimens we use neural network, genetic algorithm and multiple regression. With intelligent system we increase production of process of laser hardening, because we decrease time of process and increase topographical property of materials. Hybrid evolutionary computation is a generic, flexible, robust, and versatile method for solving complex global optimization problems and can also be used in practical applications. This paper explores the use of an intelligent system with such a hybrid method to improve existing hybrids. It describes a new hybrid method based on the cycle integration method.

**Keywords:** Artificial intelligence, visibility graphs, pattern recognition, modeling, hybrid system

## 1 INTRODUCTION

The visibility graph [1] is a fundamental geometric structure that is useful in many applications, including illumination and rendering, motion planning, pattern recognition and sensor networks. A graph  $G$  is called a visibility graph if there is a polygon  $P$ , such that the vertices of  $P$  are the vertices of  $G$  and two vertices are adjacent in  $G$  if they are visible in  $P$ . Visibility graph [2] analysis is a spatial analysis technique for urban and building spaces that may also be applied to landscapes, which was pioneered at the VR Centre. The method involves taking a selection of points across a space and forming graph edges between those points, if they are mutually visible, to form a visibility graph. Visibility graphs are widely used for 2D applications but

we are interested in their application to complex 3D visibility problems. Visibility calculations are central to any computer graphics application. We study the complex microstructure of robot laser-hardened specimens and present the microstructure in 3D space; thus, using 3D visibility graphs for describing this microstructure. Robot laser surface hardening [3] heat treatment is complementary to conventional flame or inductive hardening. The energy source for laser hardening is the laser beam which heats up very quickly and the metal surface area of ponds up to 1.5mm. In this paper, we present a new method for describing 3D visibility graphs for analysing the microstructure of robot laser-hardened specimens with new method; visibility graph in 3D space. There are many processes of hardening: inductive, flame, hardening in hardening furnaces and most importantly, robot laser hardening. Intelligent computing has attracted many scientists and researchers working on intelligent techniques for solving complex real-world problems. The aim of this contribution is to outline possibilities for applying an intelligent system method to predicting complexity of terrain surfaces with topological properties of visibility graphs of 3D space and to judge their prospective use in this field. The achieved models enable the prediction of final porosity on the basis of decisive laser beam parameters influencing these properties. By modelling this intelligent system, we will reduce the time, cost and work process, increase competitiveness and allow us to progress more rapidly in the process of heat treatment of materials and improve economic potential. Moreover, this paper explores the use of an intelligent system with such a hybrid method [4] to improve existing hybrids. It describes a new hybrid method based on the cycle integration method. In this work, we have used scanning electronic microscopy (SEM) [5] to analyse the pictures of the microstructure of the robot laser-hardened specimen. The aim of the study is to develop an algorithm for constructiong visibility graphs in 3D space for determination complexity of porosity of the microstructure of robot laser-hardened specimens. An application of the algorithm for construction of a 3D visibility graph to analyse the microstructure of the laser technique in hardening the specimen, is also illustrated in Section 3.

### **1.1 Related Work**

The visibility graph problem itself has long been studied and has been applied to a variety of areas. The first attempts to cope with the cost of visibility computations involved space partitioning structures but they provided only local visibility information. In their early survey Sutherland et al. in year 1974 classified hidden-part removal algorithms into object space and image-space methods. As opposed to classification of Sutherland et al., this plane is not restricted to the plane of the actual image. It can be an intermediate plane. Consider the example of hard shadow computation: an intermediate image from the point light source can be computed. The first visibility techniques were developed for hidden line removal in the sixties. Hershberger et al. [6] propose an algorithm for the problem of computing shortest paths among curved obstacles in the plane. Chen et al. [7] shown technique which is also applicable to a motion planning problem of finding a short-

est path to translate a convex object in the plane from one location to another avoiding a given set of polygonal obstacles, improving the previously best known solution and settling an open problem posed in 1988. Chen et al. [8] study the problem of computing an L1 (or rectilinear) shortest path between two points avoiding the obstacles. Their algorithm can also be extended to obtain improved results for other related problems, e.g., finding shortest paths with fixed orientations, finding approximate Euclidean shortest paths, etc. Chen and Wang [9, 10] consider the problem version on curved obstacles, which are commonly modeled as splinegons. Streinu [11] constructs a pseudo-visibility graph for which there exists a unique compatible vertex-edge visibility graph, which is then shown to be non-stretchable. Most of the algorithms developed in computational geometry to solve the hidden part removal problem are based on a sweep of the visibility map for polygonal scenes. In this paper, we present a new approach to constructing visibility graphs in 3D space.

## 2 MATERIALS PREPARATION AND METHOD

### 2.1 Materials Preparation

The study was undertaken using tool steel. The chemical composition of the material contained: 0.38–0.45 % C, 0.4 % maximum Si, 0.6–0.9 % Mn, 0.025 % maximum P, 0.035 % maximum S and 0.15–0.3 % Mo [12]. The specimen test section was in a cylindrical form with dimensions of 2510 mm. After hardening, we polished [13] all specimens and the test specimens were cut into smaller parts. We used a field emission scanning electron microscope, type JEOL JSM-7600F, to obtain the pictures (Figure 2) of the surface of the robot laser-hardened specimens. To analyse the pictures we used the software program ImageJ. We used the method of determining the porosity from SEM images of the microstructure. It is known that in a homogenously porous material the area of pores is equal to the volume of pores in specimens. The SEM pictures were converted to binary images (Figure 1), from which we calculated the area of pores of all pictures using the ImageJ program (ImageJ is a public domain, Java-based image processing program developed at the National Institutes of Health). The area of pores on each picture of the material was calculated and then the arithmetic mean and standard deviation of porosity were determined.

### 2.2 Method

We developed a new algorithm for the construction of visibility graphs in 3D space [14]. This algorithm was used to determination complexity of porosity of hardened specimens. Also, we use topological property of visibility graphs in 3D space; density to determinate complexity of porosity. We calculated density of visibility graphs with program Pajek. First, we analyzed the profile graph of the microstructure picture with a visibility graph. Algorithms for 2D visibility graphs already exist [15]. Two

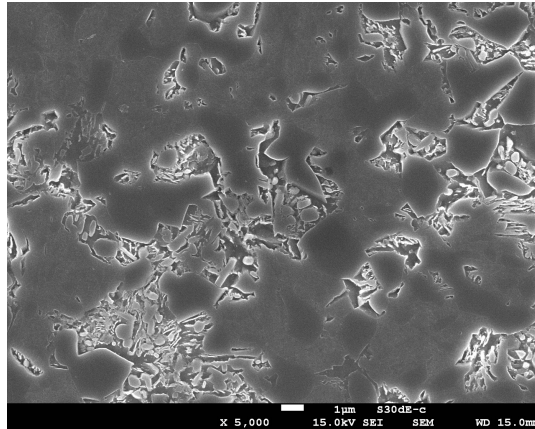


Figure 1. Microstructure of hardened tool steel

arbitrary data values  $(x_a, y_a)$  and  $(x_b, y_b)$  will have visibility, and consequently will become two connected nodes of the associated graph, if any other data  $(x_c, y_c)$  placed between them fulfills:

$$y_c < y_b + (y_a - y_b) * (x_b - x_c) / (x_b - x_a).$$

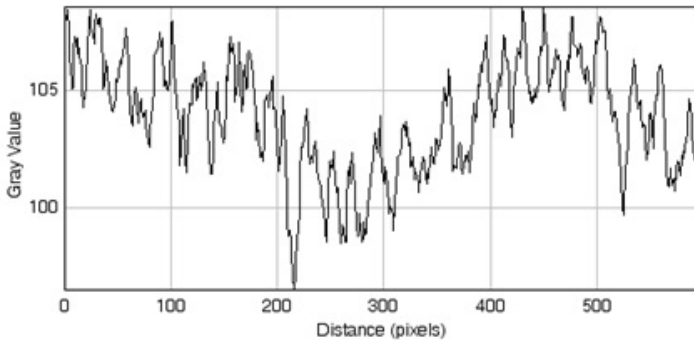


Figure 2. Profile graph of surface hardened specimen

Figure 2 presents the profile graph of microstructure in Figure 1. Figure 3 presents 2D visibility graph. The reason for developing the construction of the visibility graph in 3D space is to analyse the topographical properties of robot laser hardening. Robot laser-hardened specimens have better microstructure topographical properties after hardening. Using a 3D visibility graph we can describe the

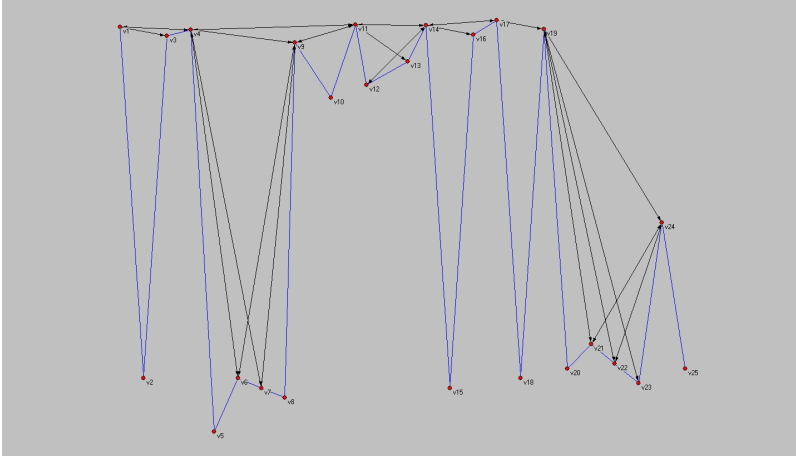


Figure 3. 2D visibility graph

complexity of the microstructure (Figure 1) of hardened specimens and we can determine those points on the graphs of the microstructure that are connected. We analysed the image format (Figure 1) with 256 gray level numerical matrices (level 1 for black and 256 for white) using the program ImageJ. Each point  $(x, y)$  of the image (2D plane) is assigned a value between 1 and 256; this value is determined by a third coordinate in the 3D coordinate system or  $z$ -coordinate. This means that the point  $T = (x, y)$  plane is given a third component and then a form of  $T_{3D} = (x, y, z)$  (Figure 4).

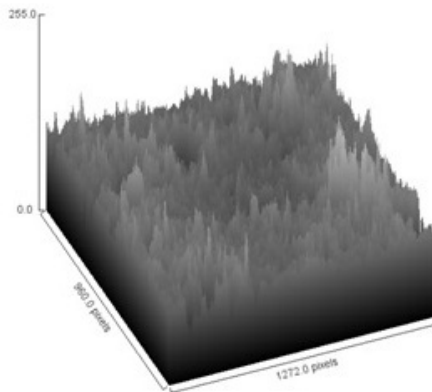


Figure 4. Three dimensional graph of hardened specimen

First, we find the maximums in Figure 5 and the extremes are presented in Figure 6 in red. We have the coordinates of all points of the 3D graphs, but we want to know which point we can connect. Some authors use different computational intelligence models, coupled with other complementary techniques, they can be used to handle problems encountered in image processing and information reasoning [16].

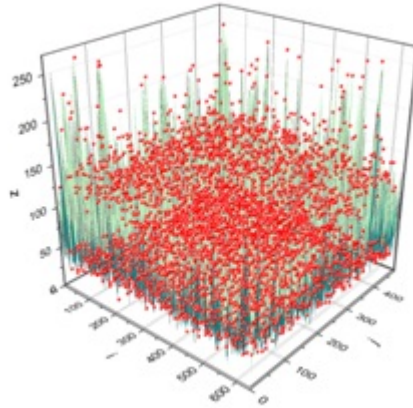


Figure 5. Extreme point (red) and all other points of graph 3 in 3D space

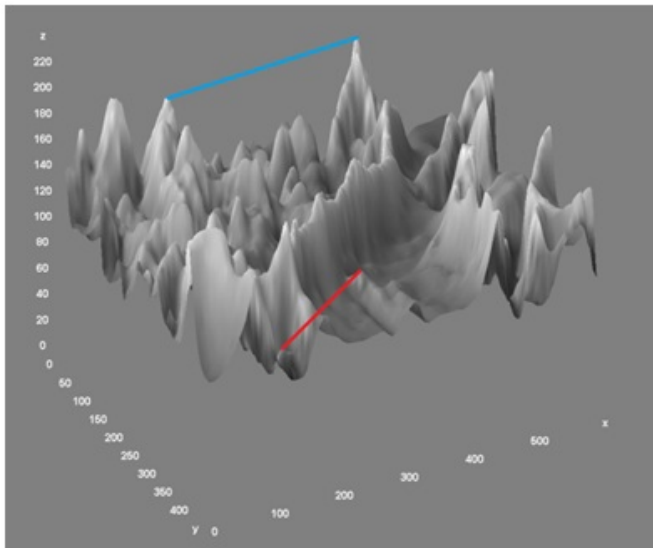


Figure 6. Visibility nodes (blue line) and unrelated nodes (red line)

### 2.3 Idea of Problem

If we do not have the coordinates of point values, then they must first be determined. We want to know how to connect the nodes in Figure 4. The coordinates  $(x, y, z)$  in Figure 4 are known and the nodes  $v_{i,j}$  and  $v_{k,l}$ , where  $i < k$ ,  $j < l$  are connected by a link, if and only, if they are visible. This means that the path from  $v_{i,j}$  to  $v_{k,l}$  has no points on the graph. An example is presented in Figure 6, in which the nodes connected by the blue line are visible to each other and the red line is an example of unrelated nodes (the straight line that connects the two nodes pierces the graph, which is contrary to the definition of a visibility graph). The following section describes how to construct a 3D visibility graph.

### 2.4 Solution of Problem

We present a graphical solution on a 5\*5 grid because it provides better visual representation. In the first step, we connect neighbouring nodes. Also, node  $T(x_i, y_j, z_{i,j})$  is connected with nodes  $T(x_{i-1}, y_j, z_{i-1,j})$ ,  $T(x_{i+1}, y_j, z_{i+1,j})$ ,  $T(x_i, y_{j+1}, z_{i,j+1})$  and  $T(x_i, y_{j-1}, z_{i,j-1})$  if node  $T(x_i, y_j, z_{i,j})$  is not located on the edge of a complex network. If node  $T(x_i, y_j, z_{i,j})$  is on the edge of a complex network, then it is connected with three or two nodes only, as presented in Figure 6. Furthermore, we have connections between  $T(x_i, y_j, z_{i,j})$  and  $T(x_{i+1}, y_j, z_{i+1,j})$ ,  $T(x_{i+1}, y_j, z_{i+1,j})$  and  $T(x_{i+1}, y_{j+1}, z_{i+1,j+1})$ ,  $T(x_{i+1}, y_{j+1}, z_{i+1,j+1})$  and  $T(x_i, y_{j+1}, z_{i,j+1})$  and  $T(x_i, y_{j+1}, z_{i,j+1})$  and  $T(x_i, y_j, z_{i,j})$ . Nodes  $T(x_i, y_j, z_{i,j})$ ,  $T(x_{i+1}, y_j, z_{i+1,j})$ ,  $T(x_{i+1}, y_{j+1}, z_{i+1,j+1})$  and  $T(x_i, y_{j+1}, z_{i,j+1})$  present quadrilaterals and it is possible to see many quadrilaterals in Figure 7.

In the second step, we present those diagonal nodes that are visible in the quadrilaterals. Nodes  $T(x_i, y_j, z_{i,j})$  and  $T(x_{i+1}, y_{j+1}, z_{i+1,j+1})$  are visible if the line through nodes  $T(x_i, y_{j+1}, z_{i,j+1})$  and  $T(x_{i+1}, y_j, z_{i+1,j})$  and the plane through the three points:  $T(x_i, y_j, z_{i,j})$ ,  $T(x_{i+1}, y_{j+1}, z_{i+1,j+1})$  and  $T(x_i, y_{j+1}, z_{i,j+1})$  have no intersection for all  $x, y \in N \cup 0$ , where  $i, j \in N$ . Nodes  $T(x_{i+1}, y_j, z_{i+1,j})$  and  $T(x_i, y_{j+1}, z_{i,j+1})$  are visible if the line through nodes  $T(x_i, y_j, z_{i,j})$  in  $T(x_{i+1}, y_j, z_{i+1,j})$  and the plane through the three points:  $T(x_i, y_j, z_{i,j})$ ,  $T(x_{i+1}, y_j, z_{i+1,j})$  and  $T(x_i, y_{j+1}, z_{i,j+1})$  have no intersection for all  $x, y \in N \cup 0$ , where  $i, j \in N$ .

In the third step, we break the set of all nodes  $(x_i, y_i, z_i)$  into two sets. The first set presents all nodes  $(x_i, 0, z_i)$  and the second set presents all nodes  $(0, y_i, z_i)$ . We present nodes that are visible in the first set and those that are visible in the second set. In the first set, two nodes:  $T_{i,j}(x_i, y_j, z_{i,j})$  and  $T_{k,l}(x_k, y_l, z_{k,l})$  are visible and consequently, they will become two connected nodes on the associated graph if any other node  $T(x_m, 0, z_{m,0})$  placed between them fulfils the relation:

$$z_{m,0} < z_{k,l} + (z_{i,j} - z_{k,l})(x_k - x_m)/(x_k - x_i).$$

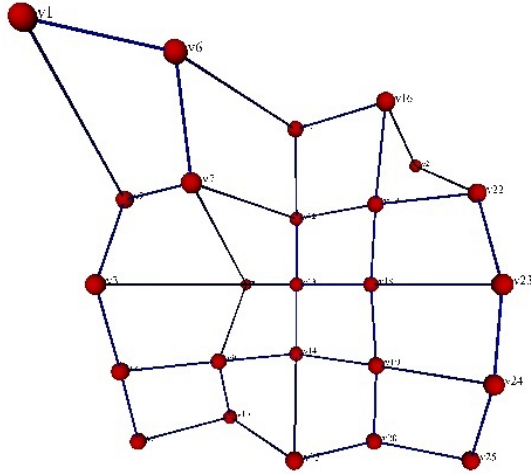


Figure 7. The first step

In the second set, two nodes:  $T_{i,j}(x_i, y_j, z_{i,j})$  and  $T_{k,l}(x_k, y_l, z_{k,l})$  are visible and consequently, they will become two connected nodes on the associated graph if any other node  $T_{0,m}(0, y_m, z_{0,m})$  placed between them fulfils the relation:

$$z_{m,0} < z_{k,l} + (z_{i,j} - z_{k,l})(y_k - y_m)/(y_k - y_i).$$

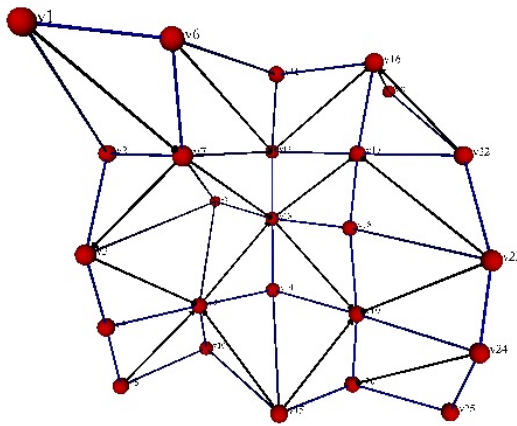


Figure 8. The second step

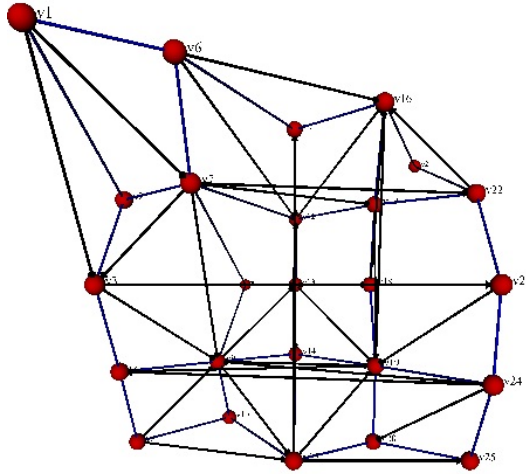


Figure 9. The third step

In the fourth step, we connect all other visible nodes. Two nodes:  $T_{i,j}(x_i, y_j, z_{i,j})$  and  $T_{k,l}(x_k, y_l, z_{k,l})$  will be visible if the line between nodes  $T_{i,j}$  and  $T_{k,l}$  and the plane through all three neighbour points, which requires the condition in step 2, have no intersection. Figure 11 presents 3D graph 5 \* 5 grid of hardened specimen.

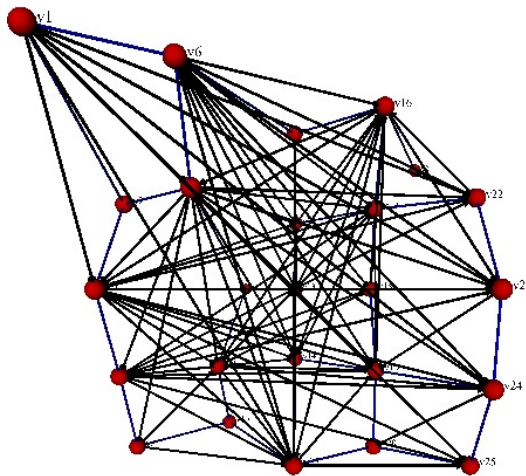


Figure 10. The fourth step

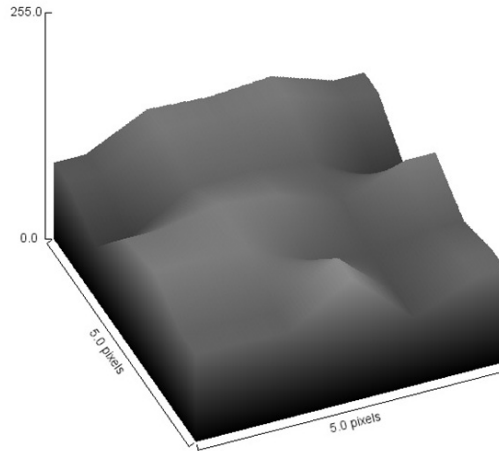


Figure 11. Example of 3D structure of hardened specimen

For modelling the results we used an intelligent system methods, namely a neural network, genetic programming method and multiple regression. We have used neural networks since the neural network is a device along the lines of biological systems – the human brain, and by using genetic programming because genetic programming is an automatically write programs following the example of natural selection (evolution). Also, those are techniques operating similarly in a human evolution. Neural networks are model-less approximators, which are capable of performing approximation modelling operations regardless of any relational knowledge of the nature of the modelled problem. The relational knowledge is typically represented by a set of equations describing the observed variables and constants that are used to describe the system's dependencies. A common use of neural networks is in multi-dimensional function modelling, i.e., the recreation of a system's behaviour on the basis of the set of known discrete points representing the various states of the system. We use feed-forward neural networks with supervised training algorithms. The basic building element of the neural network used is an artificial neural network cell (ANN) (Figure 12). In our case we use 13 data for the learn test set and 7 data for the test set. The results are presented in column Prediction with NN 35% in Table 2. In the second case, we use 10 data for the learn test set and 10 data for the test set. These results are presented in the column named Prediction with NN 50% in Table 2. In the third case, we use method one live out. Also, we use 19 data for the learn test set and 1 data for the test set.

Genetic programming [17] is a collection of methods for the automatic generation of computer programs that solve carefully specified problems, via the core, but highly abstracted principles of natural selection. The organisms that undergo adaptation are in fact mathematical expressions (models) for the surface porosity of hardened

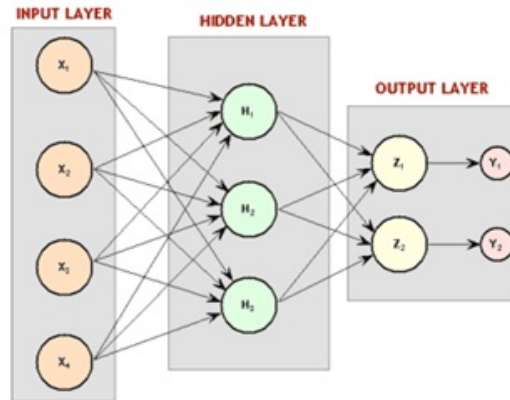


Figure 12. The general multi-layer neural network system

specimens prediction in the present work. The porosity prediction is based on the available function genes (i.e., basic arithmetical functions) and terminal genes (i.e., independent input parameters, and random floating-point constants). In the present case the models consist of the following function genes: addition (+), subtraction (-), multiplication (\*) and division (/), and the following terminal genes: air temperature in degree of Celsius [ $^{\circ}\text{C}$ ] (X1), speed of hardening [ $\text{m/s}$ ] (X2), density of 3D visibility graphs (X3), and basic porosity (X4). One of the randomly generated mathematical models –  $(X1/X4-7)*X3/2,8$  – is schematically represented in Figure 13 as a program tree with included function genes (\*, -, /) and terminal genes (X1, X2, X3 and a real number constants 7 and 2.8).

The following evolutionary parameters were selected for the process of simulated evolutions: 500 for the size of the population of organisms, 100 for the maximum number of generations, 0.4 for the reproduction probability, 0.6 for the crossover probability, 6 for the maximum permissible depth in the creation of the population, 10 for the maximum permissible depth after the operation of crossover of two organisms, and 2 for the smallest permissible depth of organisms in generating new organisms. Genetic operations of reproduction and crossover were used. For selection of organisms the tournament method with tournament size 7 was used. The analysis of covariance (generally known as ANCOVA) is a technique that sits between analysis of variance and regression analysis. Covariance is a measure of how much two variables change together and how strong the relationship is between them. ANOVA can be extended to include one or more continuous variables that predict the outcome or dependent variable. Figure 14 presents the analysis of covariance.

Hybrid evolutionary computation is a generic, flexible, robust, and versatile method for solving complex global optimisation problems and can also be used

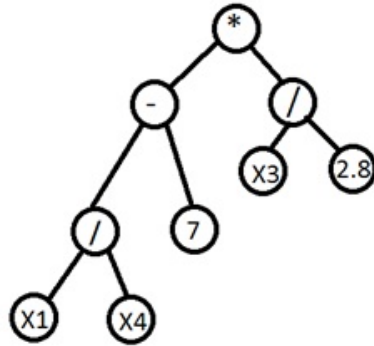


Figure 13. Randomly generated mathematical model for the surface porosity of hardened specimens prediction, represented in the program tree form

in practical applications. We present a new hybrid method based on the cycle integration method. Cyclic hybrid methods are connected in series in the direction of the entrance to the method  $n$ . All methods work independently of the other methods. The results of input method 1 are transferred to input method 2, the results of input method 2 are transferred to input method 3, and so on, the results

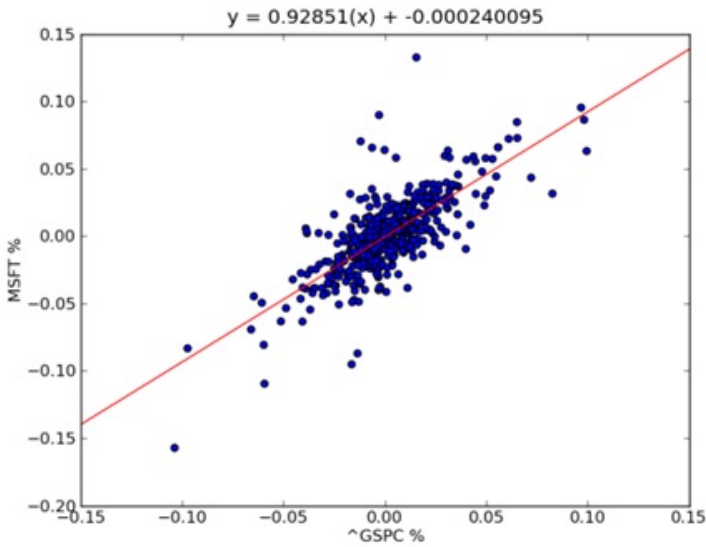


Figure 14. The analysis of covariance

of input method  $n - 1$  are transferred to the input method  $n$  and the results of input method  $n$  are transferred to input method 1. Thus, the procedure is repeated cyclically. Cycles can be performed as often as desired (Figure 15). We connect method genetic programming – regression – neural network – regression – neural network, also  $GP - R - NN - R - NN$ .

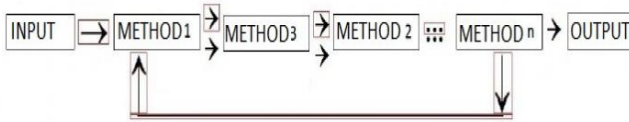


Figure 15. The cyclic hybrid method

### 3 RESULTS AND DISCUSSION

In Table 1 the parameters of hardened specimens that have an impact on porosity are presented. We mark specimens from P1 to P20. Parameter X1 presents the parameter of temperature in degree of Celsius [°C], X2 presents the speed of hardening [mm/s] and X3 presents density of visibility graphs in 3D space. The last parameter Y is the measured surface porosity of laser-hardened robot specimens. Table 2 presents experimental and prediction data regarding the surface porosity of laser-hardened robot specimens. In Table 2 the symbol S presents name of specimens, ED experimental data, NM 1 prediction with neural network with 35 % learn set, NM 2 prediction with neural network with 50 % learn set, NM 3 prediction with neural network with method one live out, R prediction with regression, G prediction with genetic programming and H prediction with new cycle integration method. In Table 1, we can see that the specimen P20 has the largest density of visibility graphs in 3D – 0.2960, thus the specimen P20 is the most complex. Specimen P20 has the most complex porosity after hardening, that is 66 %. The measured and predicted surface porosity of laser-hardened robot specimens is shown in the graph in Figure 16. The genetic programming model is presented under Model of Regression. The genetic programming model presents 9.67 % deviation from the measured data, which is less than the regression model, which presents 19.19 % deviation. The best neural network presents 6.73 % deviation from the measured data. New cyclic hybrid method presents 11.30 % deviation from the measured data, which is less than the regression model and less than neural network with 35 % and 50 %.

Model Regression:

$$Y = 106,0807 - 0,0201 * X1 - 4,366 * X2 - 112,709 * X3.$$

Model of Genetic Programming:

$$Y = 72.3303 + 0.121453 * X_1 + \frac{0.0263618 * X_1 * \left(-8.5785 + X_1 + \frac{8.5785}{x_3}\right)}{-0.11657 + \frac{167.74}{x_3^2} - \frac{8.5785-x_1}{x_3}} - \frac{2.3939 * x_1 * x_3^2 * \left(-8.5785 + X_1 + \frac{0.0263618 * X_1}{X_3}\right) - 8.5785 * x_3^2 - 8.5785 * x_3^3}{\left(-3207.59 - 0.11657 * X_1 + \frac{X_1}{X_3} - 8.5785 * X_3\right) * (-7.08381 + X_3)} - \frac{0.0115654 * \left(X_1 - 8.43158 * \left(X_2 + \frac{1.23398 * X_2}{7.08381 + X_3}\right)\right)}{X_3^2 * \left(72.3303 - 0.11657 * X_1 + \frac{1.70206 * (-79.672 + X_1) * (-7.08381 + X_3) + \left(-8.5785 + \frac{X_3^2}{X_2}\right)}{X_3 * \left(-0.11657 * X_1 + \frac{98.3133}{X_1 * X_3} - 75.8603 * (-7.08381 + X_3) * X - 3^2\right)}\right)}$$

$P_i$	$X_1$ [°C]	$X_2$ [mm/s]	$X_3$	Y [%]
P1	1000	2	0.1936	46
P2	1000	3	0.2208	45
P3	1000	4	0.2144	43
P4	1000	5	0.2256	41
P5	1400	2	0.2445	36
P6	1400	3	0.2221	49
P7	1400	4	0.2036	45
P8	1400	5	0.2096	48
P9	1000	2	0.2352	46
P10	1000	3	0.2288	32
P11	1000	4	0.2144	45
P12	1000	5	0.2352	42
P13	1400	2	0.2208	28
P14	1400	3	0.2320	19
P15	1400	4	0.1984	41
P16	1400	5	0.1904	38
P17	800	0	0.2832	47
P18	1400	0	0.2688	52
P19	2000	0	0.2416	50
P20	950	0	0.2960	66

Table 1. Parameters of robot laser-hardened specimens

### 3.1 Discussion

We use visibility graphs to describe topographical properties of the hardened specimens. Visibility graphs of a series of digitized surface microstructures from the surface of the robot-laser-modified specimens indicate that useful correlations can be derived between the topological properties of 3D visibility graphs and the surface

S	ED	NM 35 %	NM 50 %	NM 95 %	R	GP	H
P1	46	46.3055	46.8231	43.8577	56.6889	43.6033	46.9226
P2	45	45.5105	42.5350	43.7115	56.7106	44.7239	48.0127
P3	43	43.0889	43.2772	43.7115	53.6983	43.5151	45.1963
P4	41	41.1525	44.0881	43.7115	50.8479	45.9593	48.3114
P5	36	36.5906	41.0196	43.7115	50.6491	36.7779	42.5353
P6	49	48.8627	43.9619	43.7115	51.1877	44.9926	49.4664
P7	45	44.6597	44.3072	43.7115	47.5332	43.5976	39.6623
P8	48	47.9322	45.9758	43.7115	46.3851	46.6678	41.2789
P9	46	61.8615	41.0944	43.6251	51.5609	39.0206	38.4699
P10	32	62.2293	38.5204	31.6252	44.2957	42.6917	32.2851
P11	45	61.7153	43.6073	43.7115	47.8452	40.9755	46.3398
P12	42	61.6377	43.4968	43.7115	43.1569	41.7638	33.9977
P13	28	62.1118	42.1813	25.9115	44.8510	39.1935	35.6465
P14	19	49.6537	31.1093	22.0631	24.0318	19.0611	24.9199
P15	41	62.2071	44.0992	43.7115	40.9921	40.8886	39.5771
P16	38	62.1229	40.3349	38.1371	31.1197	40.0856	27.2034
P17	47	47.2896	38.7641	53.8123	67.4936	50.1034	58.8769
P18	52	43.2661	40.3948	50.3781	58.1676	50.2104	49.4343
P19	50	33.7480	41.5247	46.9130	48.1570	50.1024	41.1488
P20	50	47.0703	83.4722	65.8783	62.9172	64.9245	48.9076

Table 2. The measured and predicted surface porosity of robot laser-hardened specimens

microstructure features such as complexity of porosity. The surface of the hardened material exhibits a more complex network than at depth, which is to be expected, because the laser beam is focused directly on the surface. Porosity is a good predictor of the performance of a mechanical component, since irregularities in the surface may form nucleation sites for cracks or corrosion. Also, we use three methods of intelligent system to make prediction of porosity of robot laser-hardened specimens. We show that the genetic programming model gives us the best predicted results. The neural network model is better than the regression model and as good as the genetic programming model. In both models, genetic programming and regression model, the coefficient of density of visibility graph has the large impact. A statistically significant relationship was found between porosity, the parameters of the robot laser cell and the topological property of visibility graphs in 3D. In addition, image analysis of SEM images of robot laser-hardened specimens is an interesting approach.

#### 4 CONCLUSION

The visibility graph problem itself has been long studied in computational geometry and was applied to a variety of areas. 3D visibility graphs can be used in many 3D geometric problems. Finally, in this work the visibility network in 3D space, which contains more information than the visibility graph, has been used to analyse

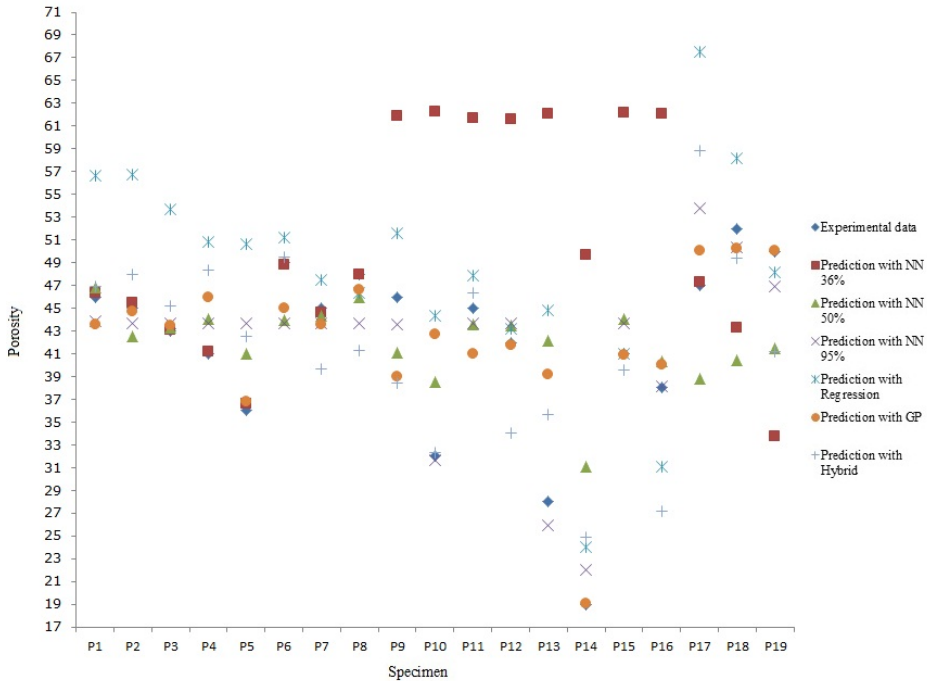


Figure 16. The measured and predicted surface porosity of robot laser-hardened specimens

the microstructure of robot laser-hardened specimens. This algorithm is also useful in many other cases, including: illumination and rendering, motion planning, pattern recognition, computer graphics, computational geometry and sensor networks. Furthermore, we use the new method of construction of the visibility graphs in 3D space to describe the topographic properties of the hardened specimens. The main findings can be summarised as follows:

1. We derived a construction of visibility graphs in 3D space.
2. There exists a complex structure in the robot laser-hardened specimens.
3. We describe the topographic properties of the hardened specimens by using the topological properties of the visibility graphs in 3D space.
4. We describe the relationship between complexity of porosity and the parameters of the robot laser cell by using the topological properties of the 3D visibility graphs. This finding is important with regard to certain alloys that are hard to mix because they have different melting temperatures; however, such alloys have better technical characteristics. By varying different parameters (e.g., temperature), robot laser cells produce different patterns with different topological properties of 3D visibility graphs.

5. For prediction of porosity of hardened specimens we use neural network, genetic algorithm and multiple regression.
6. The genetic programming modelling results show good agreement with measured porosity of hardened specimens.
7. We develop a new hybrid method of prediction with an intelligent system.
8. With intelligent system we increase production of process of laser hardening, because we decrease time of process and increase topographical property of materials.

### Acknowledgement

This work is supported by projects VEGA 2/0167/16, EU H2020-777533 PROCESS, EU H2020-777435 DEEP-HybridDataCloud.

### REFERENCES

- [1] BABBITT, M.: On Visibility Graphs – Upper Bounds and Classification of Special Types. Research Science Institute (RSI) Mathematics Section Abstracts of Final Research Papers, M.I.T., Summer 2012.
- [2] BABBITT, M.—GENESON, J. T.—KHOVANOVA, T.: On  $k$ -Visibility Graphs. 2014, <https://arxiv.org/pdf/1305.0505.pdf>.
- [3] BABIČ, M.—BALIČ, J.—KOKOL, P.: Optimal Fractal Dimension on Grain Structure Robot Laser-Hardened Tool Steel. *Advances in Production Engineering and Management*, ISSN 1854-6250, Vol. 9, 2014, No. 3, pp. 119–127, doi: 10.14743/apem2014.3.181.
- [4] RAVI, V.—NAVEEN, N.—PANDEY, M.: Hybrid Classification and Regression Models via Particle Swarm Optimization Auto Associative Neural Network Based Nonlinear PCA. *International Journal of Hybrid Intelligent Systems*, Vol. 10, 2013, No. 3, pp. 137–149, doi: 10.3233/HIS-130173.
- [5] TAHMASEBI, P.—SAHIMI, M.: Reconstruction of Three-Dimensional Porous Media Using a Single Thin Section. *Physical Review E*, Vol. 85, 2012, No. 6, Art. No. 066709, doi: 10.1103/PhysRevE.85.066709.
- [6] HERSHBERGER, J.—SURI, S.—YILDIZ, H.: A Near-Optimal Algorithm for Shortest Paths among Curved Obstacles in the Plane. *Proceedings of the Twenty-Ninth Annual Symposium on Computational Geometry (SoCG '13)*, Rio de Janeiro, Brazil, 2013, pp. 359–368, doi: 10.1145/2462356.2462374.
- [7] CHEN, D. Z.—HERSHBERGER, J.—WANG, H.: Computing Shortest Paths amid Convex Pseudodisks. *SIAM Journal on Computing*, Vol. 42, 2013, No. 3, pp. 1158–1184, doi: 10.1137/110840030.
- [8] CHEN, D. Z.—WANG, H.: A Nearly Optimal Algorithm for Finding L1 Shortest Paths among Polygonal Obstacles in the Plane. *Proceedings of the 19<sup>th</sup> European Conference on Algorithms (ESA '11)*, Saarbrücken, Germany, 2011, pp. 481–492.

- [9] CHEN, D.Z.—WANG, H.: Computing Shortest Paths among Curved Obstacles in the Plane. *ACM Transactions on Algorithms*, Vol. 11, 2015, Art.No. 26, doi: 10.1145/2660771.
- [10] CHEN, D.Z.—WANG, H.: Visibility and Ray Shooting Queries in Polygonal Domains. *Computational Geometry*, Vol. 48, 2015, No. 2, pp. 31–41.
- [11] STREINU, I.: Non-Stretchable Pseudo-Visibility Graphs. *Computational Geometry*, Vol. 31, 2005, No. 3, pp. 195–206, doi: 10.1016/j.comgeo.2004.12.003.
- [12] European Steel and Alloy Grades, 2011–2013, <http://www.splav.kharkov.com/steelgrade/>.
- [13] GUO, Y.—ZHANG, Y.—HUANG, H.—MENG, X.—LIU, Y.—TU, S.—LI, B.: Novel Glass Ceramic Foams Materials Based on Polishing Porcelain Waste Using the Carbon Ash Waste as Foaming Agent. *Construction and Building Materials*, Vol. 125, 2016, pp. 1093–1100, doi: 10.1016/j.conbuildmat.2016.08.134.
- [14] BABIČ, M.: Analysis of Hardened Materials Using Fractal Geometry (in Slovenian). Dissertation, University of Maribor, 2014, 164 pp.
- [15] LACASA, L.—LUQUE, B.—BALLESTEROS, F.—LUQUE, J.—NUÑO, J.C.: From Time Series to Complex Networks: The Visibility Graph. *Proceedings of the National Academy of Sciences USA*, Vol. 105, 2008, No. 13, pp. 4972–4975.
- [16] LIM, C.P.—ABEYNAYAKE, C.—SATO-ILIC, M.—JAIN, L.C.: Special Issue: Computational Intelligence Models for Image Processing and Information Reasoning. *Journal of Intelligent and Fuzzy Systems*, Vol. 24, 2013, No. 2, pp. 199–200.
- [17] GAUCEL, S.—KEIZER, M.—LUTTON, E.—TONDA, A.: Learning Dynamical Systems Using Standard Symbolic Regression. *Genetic Programming (EuroGP 2014)*. Springer, Berlin, Heidelberg, Lecture Notes in Computer Science, Vol. 8599, 2014, pp. 25–36, <http://evelyne.lutton.free.fr/Papers/evostar-2014-differential-equations.pdf>.

**Matej BABIČ** received his Ph.D. degree in computer science from the Faculty of Electrical Engineering and Computer Science, University of Maribor, Slovenia, and is currently PostDoc Researcher in the Jozef Stefan Institute. He studied mathematics at the Faculty of Education in Maribor. His research interest is in fractal geometry, graph theory, network, intelligent systems, hybrid machine learning and topography of materials after hardening.

**Ladislav HLUCHÝ** is the Vice-Director of the Institute of Informatics, Slovak Academy of Sciences and also the Head of the Department of Parallel and Distributed Computing at the Institute. He received his M.Sc. and Ph.D. degrees, both in computer science. He is R&D Project Manager, Work-Package Leader in a number of 4FP, 5FP and 6FP projects, as well as in Slovak R&D projects (VEGA, APVT, SPVV). He is a member of IEEE, ERCIM, SRCIM, and EuroMicro consortiums, Editor-in-Chief of the journal *Computing and Informatics*. He is (co-)author of scientific books and numerous scientific papers, contributions and invited lectures at international scientific conferences and workshops. He also gives lectures at the Slovak University of Technology, Bratislava, Slovakia. He is a supervisor and consultant for Ph.D., master and bachelor studies.

**Peter KRAMMER** graduated from the Faculty of Electrical Engineering and Information Technology, Slovak University of Technology in Bratislava, and is currently Researcher at the Institute of Informatics, Slovak Academy of Sciences. His research interests include data mining and machine learning. He is (co-)author of several scientific papers and has participated in international and national research projects.

**Branko MATOVIČ** received his Dr. Rer. Nat. degree from Max-Planck Institute Stuttgart and University Stuttgart. He is Director of Centre of Excellence-CEXTREME MAT, Vinča Institute of Nuclear Sciences, Belgrade University. Presently his main interest includes nonconventional synthesis methods for oxide and non-oxide powders, synthesis and densification of oxide and non-oxide ceramics, densification, phase transformations and crystal growth during temperature-pressure treatments and material characterization. Especially he works in area of a nanostructured design of new materials for application in extreme environments.

**Ravi KUMAR** received his doctorate in natural sciences from the Max Planck Institute for Metals Research (currently known as Max Planck Institute for Intelligent Systems), Stuttgart, Germany in 2004 with a “Sehr gut” grade (very good) with a fellowship from the Max Planck Institute. Subsequently, he continued in the same institute as PostDoctoral Researcher and Guest Scientist. He worked on the high temperature deformation behavior of polymer precursor derived ceramics during his stay. After 6 years of stay at the Max Planck Institute, he moved to the Institute for Shock Physics in Pullman, USA and worked on the dynamic response of bulk metallic glasses for a brief period. He returned back to India in 2007 and joined the Department of Metallurgical and Materials Engineering, at IIT Madras as Associate Professor. Since 2012, he is working in the same department as Associate Professor and heads the Central XRD Laboratory. As the Head of the Central XRD Laboratory he provides consulting to a large number of industries.

**Pavel KOVAČ** received his B.Sc., M.Sc. and Ph.D. degrees from the University of Novi Sad, Serbia, in 1975, 1980 and 1987, respectively. He is currently Full Professor at the Faculty of Technical Sciences, University of Novi Sad, Serbia. He is the Chair for Chip Removal Technologies and Chief Editor of Journal for Production Engineering. He is a member of the International Technology Management Academy in Novi Sad. His research interests include machining technology, metal cutting and high productive technologies, ecological systems and technologies, plastics and environment, design of experiment and artificial intelligence.